Spectrochimica Acta Part B 63 (2008) 962–967

Contents lists available at ScienceDirect

Spectrochimica Acta Part B

journal homepage: www.elsevier.com/locate/sab

Fast and accurate expression for the Voigt function. Application to the determination of uranium M linewidths

Silvina P. Limandri [a,b], Rita D. Bonetto [b,c], Héctor O. Di Rocco [b,d], Jorge C. Trincavelli [a,b,*]

[a] Facultad de Matemática, Astronomía y Física, Universidad Nacional de Córdoba, Ciudad Universitaria, 5000, Córdoba, Argentina
[b] Consejo Nacional de Investigaciones Científicas y Técnicas de la República Argentina
[c] Centro de Investigación y Desarrollo en Ciencias Aplicadas Dr. Jorge Ronco, Calle 47 No 257, 1900 La Plata, Argentina; Facultad de Ciencias Exactas y Facultad de Ingeniería de la UNLP, La Plata, Argentina
[d] Instituto de Física Arroyo Seco, Facultad de Ciencias Exactas, Universidad Nacional del Centro, Pinto 399, 7000 Tandil, Argentina

ARTICLE INFO

Article history:
Received 28 November 2007
Accepted 6 June 2008
Available online 13 June 2008

Keywords:
Voigt function
Natural linewidths
Uranium M characteristic lines
EPMA

ABSTRACT

The Voigt function is the convolution between a Gaussian and a Lorentzian distribution. The numerical implementation of this function is required in diverse areas of physics and applied mathematics. An explicit representation for the Voigt function is developed in terms of series of trigonometric and hyperbolic functions. The obtained expression permits a very fast evaluation of Voigt profiles with a degree of accuracy higher than the one required for spectroscopy applications. In addition, this expression is implemented in a numerical algorithm of parameter optimization in electron probe microanalysis, and applied to determine natural linewidths for several transitions to the uranium M levels.

1. Introduction

The importance of the Voigt function $V(x)$ arises in several fields of physics and applied mathematics. This function is the convolution of two probability distributions: a Gaussian $G(x)$ and a Lorentzian $L(x)$. It is very useful in the study of stellar atmospheres, X-ray and plasma spectroscopies, physics of nuclear-fission reactors, etc.

Particularly, in atomic physics, several relative transition probabilities and natural linewidths, which are related to the lifetime of the corresponding decays, require accurate determinations due to the large discrepancy among the different data published. The application of the Voigt function in this field permits to describe the characteristic line profiles in a realistic way, because they involve a Gaussian contribution due to instrumental features and a Lorentzian component intrinsic of the nature of the emission process.

Due to the lack of a closed-form expression for the Voigt function, the pseudo-Voigt function is a usual approach in X-ray spectroscopy [1–4]. This function is a linear combination of a Gaussian and a Lorentzian. In order to avoid this approach, a number of attempts were done; for instance, an empirical approximation was published by Liu et al. [5]. Previously, other approximation to the standardized Voigt function was made by Kielkopf [6] and computational procedures were reviewed by Drayson [7]. Thompson [8] summarized diverse types of approximations to $V(x)$ and Brablec et al. [9] proposed a general deconvolution method based in the B-splines for the related inversion problem, and comment a specific application to $V(x)$. Recently, an expression based in the power series expansion for the Voigt function, was developed [10]. The expression for $V(x)$ given in Eq. (14) of that publication, based in the solution of a first order differential equation, is erroneous, since $V(x)$ satisfies a non-homogeneous second order differential equation; nevertheless, the power series expansion in terms of the Kummer functions given by Eqs. (6) and (7) of the same article, is correct, as deduced in a previous publication [11].

In this work, the proper second order differential equation is considered to achieve a simple expression to describe the Voigt function. The evaluation of the obtained formula requires less computational time than previous algorithms keeping a degree of accuracy higher than the one required for spectroscopic applications. It is important to rely on a rapid and accurate method when hundred of millions of evaluations are required; for instance, in the case of certain iterative algorithms for spectral fitting, or in the study of stellar atmospheres, where thousands of spectral lines are simulated with multiple atmospheric layers at different temperatures and pressures.

The expression obtained is implemented in a numerical algorithm of parameter optimization in electron probe microanalysis, and applied to determine natural linewidths for several transitions to the uranium M levels.

* Corresponding author. Facultad de Matemática, Astronomía y Física, Universidad Nacional de Córdoba, Ciudad Universitaria, 5000, Córdoba, Argentina.
E-mail address: jorge@quechua.fis.uncor.edu (J.C. Trincavelli).

0584-8547/$ – see front matter © 2008 Elsevier B.V. All rights reserved.
doi:10.1016/j.sab.2008.06.001

2. Implementation of a new expression for the Voigt function

In view of the different nomenclatures used for the Gaussian, Lorentzian and Voigt functions and the parameters related to them, it is useful to remark the conventions followed in the present work. All these functions will be normalized to unity:

$$\int_{-\infty}^{\infty} P(x)\mathrm{d}x = 1$$

where x is the independent variable (wavelength, energy, etc.) and P refers to the function of interest. The half width at half maximum will be denoted by γ and the subindexes G, L and V, indicate Gaussian, Lorentzian and Voigt, respectively.

With the above conventions, the normalized distributions are:

$$G(x) = \frac{\sqrt{\ln 2}}{\sqrt{\pi}\gamma_G}\exp\left[-\ln 2(x/\gamma_G)^2\right] \tag{1}$$

and

$$L(x) = \frac{1}{\pi\gamma_L}\frac{\gamma_L^2}{(x^2+\gamma_L^2)} \tag{2}$$

therefore

$$V(x) = \frac{\sqrt{\ln 2}\gamma_L}{\pi^{3/2}\gamma_G}\int_{-\infty}^{\infty}\frac{\exp\left[-\ln 2(x'/\gamma_G)^2\right]}{(x-x')^2+\gamma_L^2}\mathrm{d}x' \tag{3}$$

By defining the dimensionless parameter a as:

$$a = \sqrt{\ln 2}\gamma_L/\gamma_G \tag{4}$$

and the dimensionless variables y and b as:

$$y = \sqrt{\ln 2}x'/\gamma_G; \quad b = \sqrt{\ln 2}x/\gamma_G \tag{5}$$

Eq. (3) can be rewritten in the form:

$$V(a,b) = \frac{a^2}{\gamma_L\pi^{3/2}}\int_{-\infty}^{\infty}\frac{\exp(-y^2)}{(y-b)^2+a^2}\mathrm{d}y \tag{6}$$

According to previous publications [12,13], taking the derivative of Eq. (6), the following second order differential equation is obtained:

$$\frac{\mathrm{d}^2V(a,b)}{\mathrm{d}b^2} + 4b\frac{\mathrm{d}V(a,b)}{\mathrm{d}b} + \left[4b^2+2(2a^2+1)\right]V(a,b) = \frac{4a^2}{\pi\gamma_L} \tag{7}$$

The solution of Eq. (7), given by Roston and Obaid [12], results:

$$V(a,b) = \frac{a}{\gamma_L\sqrt{\pi}}\left\{e^{a^2-b^2}\mathrm{erfc}(a)\cos(2ab) - \frac{2}{\sqrt{\pi}}e^{-b^2}\left[\cos(2ab)\int_0^b e^{u^2}\sin(2au)du - \sin(2ab)\int_0^b e^{u^2}\cos(2au)du\right]\right\} \tag{8}$$

where erfc denotes the complementary error function. In order to overcome the inefficiency of using two integrals, the use of simple trigonometric identities leads to a more suitable expression of Eq. (8), written in terms of one integral, as has been expressed by Zaghloul [14]:

$$V(a,b) = \frac{a}{\gamma_L\sqrt{\pi}}\left\{e^{a^2-b^2}\mathrm{erfc}(a)\cos(2ab) + \frac{2}{\sqrt{\pi}}\int_0^b e^{-(b^2-u^2)}\sin\left[2a(b-u)\right]\mathrm{d}u\right\} \tag{9}$$

In the present work, an alternative strategy was followed; the integrals in Eq. (8) were expressed in terms of the error function erf with complex argument, as shown in the following equation:

$$V(a,b) = \frac{ae^{a^2-b^2}}{\gamma_L\sqrt{\pi}}\left\{\mathrm{erfc}(a)\cos(2ab) + \cos(2ab)[\mathrm{erf}(a) - \mathrm{Re}(\mathrm{erf}(a+ib))] + \sin(2ab)[\mathrm{Im}(\mathrm{erf}(a+ib))]\right\} \tag{10}$$

Eq. (10) does not explicitly involve integrals, but it is expressed in terms of the error function, which is available in many software packages. If an expression in terms of real arguments is required, an infinite series approximation for the error function with complex argument can be used; for instance, the expansion given by Abramowitz and Stegun [15]:

$$\mathrm{erf}(a+ib) = \mathrm{erf}(a) + \frac{\exp(-a^2)}{2\pi a}\left[(1-\cos(2ab)) + i\sin(2ab)\right] + \frac{2}{\pi}\exp(-a^2)\sum_{n=1}^{\infty}\frac{\exp(-n^2/4)}{n^2+4a^2}\left[f_n(a,b)+ig_n(a,b)\right] + \varepsilon(a,b)$$

where

$$f_n(a,b) = 2a - 2a\cosh(nb)\cos(2ab) + n\sinh(nb)\sin(2ab)$$
$$g_n(a,b) = 2a\cosh(nb)\sin(2ab) + n\sinh(nb)\cos(2ab)$$
$$|\varepsilon(a,b)| \approx 10^{-16}|\mathrm{erf}(a+ib)|$$

which, in turn, allows us to express Eq. (10) as:

$$V(a,b) = \frac{a\exp(-b^2)}{\gamma_L\sqrt{\pi}}\left\{\mathrm{erfc}(a)\exp(a^2)\cos(2ab) + \frac{1}{2\pi a}(1-\cos(2ab)) + \frac{2}{\pi}\sum_{n=1}^{\infty}\frac{\exp(-n^2/4)}{n^2+4a^2}\left[g_n(a,b)\sin(2ab) - f_n(a,b)\cos(2ab)\right]\right\} \tag{11}$$

The product $\mathrm{erfc}(a)\exp(a^2)$ must be carefully evaluated, since it can lead to overflow/underflow errors for large values of a. To this end, the expression proposed by Cody [16] was used (see Appendix A). The uncertainty level of this expression is very low, relative errors being less than 10^{-18} in the a range indicated by the author. In this work, the lower limit for the parameter a was extended from 0.46875 down to 0.01 keeping an accuracy of the order of 10^{-12}.

The Voigt function was implemented in the software POEMA developed for electron probe microanalysis (EPMA) for the optimization of atomic and experimental parameters [17]. With this purpose, Eq. (11) was used for $b<75$, while for greater values of b, the asymptotic expansion given by Di Rocco and Aguirre Téllez [18]:

$$V(a,b) \sim \frac{a^2}{\pi\gamma_L(a^2+b^2)}\left\{1 - \frac{\cos[3\arctan(b/a)]}{2(a^2+b^2)\cos[\arctan(b/a)]}\right\} \tag{12}$$

was adopted, because it results sufficiently accurate (see below).

The method of optimization consists in minimizing the differences between an experimental spectrum and an analytical function proposed to predict it. This function takes into account characteristic peaks, bremsstrahlung and different detection artifacts. Thus, the quantity to be minimized is:

$$\chi^2 = \frac{1}{N-P}\sum_i\frac{\left(\tilde{I}_i - I_i\right)^2}{I_i} \tag{13}$$

where N is the number of channels in the spectral region of interest, P is the number of parameters fitted, $\tilde{I}_i$ and I_i are respectively the predicted and experimental intensities for the energy E_i of the channel i.

3. Experimental

Measurements were performed with a scanning electron microscope LEO 1450VP at the Laboratorio de Microscopía Electrónica y

Microanálisis (LABMEM) of the Universidad Nacional de San Luis. This equipment is furnished with a wavelength dispersive spectrometer (WDS) INCAWAVE 700. The arrangement of the WDS system is Johansson type for the crystal used in this work. The photons diffracted by the analyzing crystal are collected by two proportional counters operated in tandem: the first of them is a P10 (90%Ar–10% CH4) flow counter and the second one is a sealed Xe counter.

The M X-ray spectrum from a uranium pure standard was collected by using a PET crystal with a slit size of 0.1 mm, within an energy range from 2.36 to 5.00 keV, at 15 kV and a beam current of 186 nA. The take-off angle and the acquisition time were 29° and 53 min, respectively. The variation of the number of collected photons produced by fluctuations in the beam current was taken into account by normalizing the spectrum with the specimen current measured at different wavelength values.

The instrumental resolution σ is governed by the angular divergence $\Delta\theta$ of the analyzer crystal and it can be derived from the Bragg's law:

$$\sigma = \frac{\gamma_G}{\sqrt{2\ln 2}} = \Delta\theta E\sqrt{\left(\frac{2d}{hc}E\right)^2 - 1} \quad (14)$$

where d is the interplanar spacing of the crystal, h is the Planck constant and c is the speed of light in vacuum. Eq. (14) is a lower limit for the instrumental resolution, since defocusing problems and, at a lower extent, the width of the rocking curve of the crystal, contributes to the experimental peak broadening [19].

4. Results and discussion

4.1. Comparison between Voigt and pseudo-Voigt profiles

Although the pseudo-Voigt function has largely been used as an approximated expression to depict the characteristic line profiles [1,2], it may lead to discrepancies too large in some cases. Fig. 1 shows an example where experimental data corresponding to the uranium Mβ line were fitted by using a Voigt profile as well as a pseudo-Voigt profile. The satellite band at the high energy side was fitted with a pure Gaussian function. The goodness of fit, related to the parameter χ^2, given in Eq. (13), was similar in both cases, which indicates that a good agreement was achieved with both strategies. Nevertheless, both approaches lead to different results for the characteristic widths. The $2\gamma_L$ value obtained using the Voigt profile (4.78 eV) is much closer to other experimental (between 3.6 and 4.3 eV — see Refs. [20–22]) and theoretical (4.7 eV — calculated according to Refs. [23,24]) data than the one obtained by means of a pseudo-Voigt approximation (6.12 eV).

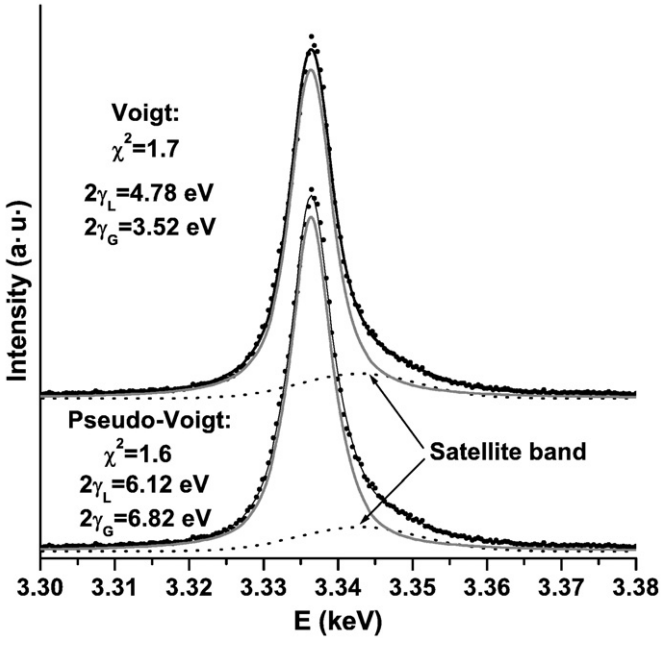

Fig. 1. Uranium Mβ line fitted with a Voigt function (up) and with a pseudo-Voigt function (down). Dots: experimental, black solid line: prediction, grey solid line: parent line and dotted line: satellite band.

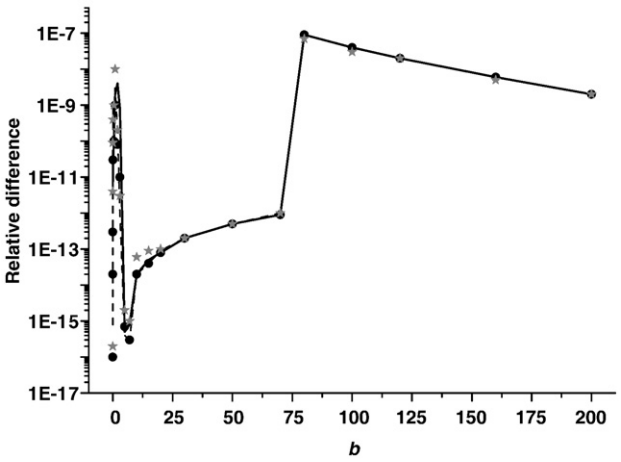

Fig. 2. Relative differences between the results obtained by Eqs. (11) and (12) and the ones given by Zaghloul [14] for a=0.01 (solid line), 0.5 (circles), 5 (dotted line) and 15 (stars).

Bearing in mind that the pseudo-Voigt profile PV can be expressed as:

$$\mathrm{PV}(x) = wG(x) + (1-w)L(x)$$

it is important to note that this profile involves, besides the widths γ_L and γ_G, a weighting factor w (0.212 in the present example). This additional parameter permits to perform a good fit, but the resulting widths lack of physical meaning. This fact may not be very significant in several situations, but leads to a misinterpretation of the spectra when atomic or experimental parameters need to be determined. For instance, in X-ray spectroscopy, the Lorentzian width corresponding to a characteristic line is related to the life time of the hole in the initial state and the Gaussian width corresponds to instrumental broadening. Another example is the study of stellar atmospheres, were γ_L and γ_G are mainly related to pressure effects and Doppler broadening, respectively.

4.2. Performance of the expression given for the Voigt function

In order to properly match experimental spectra with fitting parameters that keep physical significance, the use of a Voigt profile becomes essential. The expression presented in Eqs. (11) and (12) is very useful, since it is easy to implement in any spectral analysis procedure. To evaluate the performance of this expression, a values within 0.01 and 15 were considered, and the domain of b was taken between 0 and 200. The Voigt function for $a<0.01$ may be considered as a pure Gaussian, whereas for $a>15$, as a pure Lorentzian, with the degree of accuracy required for several spectroscopic applications. On the other hand, within the studied a range, for $b>200$, the Voigt function takes values between 10^2 and 10^6 times lower than its maximum value, which is usually comparable to the statistical fluctuations.

The precision of the present method was compared with the results published by Zaghloul [14], since the data published by this author have relative errors very low ($<10^{-13}$) within the a and b domains studied here. In order to perform the comparison, it was necessary to multiply Eqs. (11) and (12) by the scale factor $\sqrt{\pi}\gamma_L/a$,

Table 1
Number N of terms used in the assessment of the series in Eq. (11) for each b range. The mean time required per evaluation of the Voigt function is also indicated

N	b range	Time per evaluation (μs)*
15	[0,3]	24
50	(3,20]	73
110	(20,50]	155
150	(50,75]	211
Asymptotic expansion	(75,∞)	0.1

*Calculations were carried out by means of a 1.60 GHz AMD Sempron microprocessor with 512 MB RAM.

since these equations are normalized to unity. The relative differences between both methods are plotted in Fig. 2. The gap observed at $b=75$ is due to the asymptotic approach – Eq. (12) – assumed above this value of b.

To obtain the accuracy shown in Fig. 2, the series in Eq. (11) was summed up to a value N which depends on the b range. The N values, as well as the corresponding average time to perform one evaluation of the Voigt function, are presented in Table 1. The last raw shows the range of b for which the asymptotic approximation – Eq. (12) – is used.

The time per evaluation of the present algorithm is much shorter than the one reported by Zaghloul [14] — of the order of milliseconds. The relative error of the present method in the less favorable case is 9×10^{-8}, which is two, four or five orders of magnitude lower than those obtained by the methods reported by Letchworth and Benner [25], Dryson [7] and Hui et al. [26], respectively.

4.3. Determination of uranium M natural linewidths

The measured uranium spectrum is shown in Fig. 3 along with the fit performed by means of the POEMA program [17]. As can be seen, the agreement is very good in the whole energy range studied. The fit was obtained using the models for characteristic and bremsstrahlung generation and attenuation detailed in a previous work and references therein [27]. The spectrometer efficiency was determined by means of a method based on the comparison of two experimental spectra: one of them measured with an energy dispersive spectrometer, and the other one, with the wavelength dispersive spectrometer whose efficiency is to be determined [28].

Table 2
Natural linewidths in eV corresponding to 12 different M uranium transitions

Lines	This work	Ref. [20]	Ref. [21]	Ref. [22]	Calc. [23,24]
M_1–N_2	56±2				
M_2–N_1	9.6±0.6				
M_2–N_4	18±1	18.1±0.2			24.4
M_3–N_1	17.0±0.5	20.2±0.8			24.4
M_3–N_5 (Mγ)	11.1±0.3[a]		14[c]		
M_3–O_5	8±1[b]	8.2±0.1			
M_4–N_2	9.9±0.4	15±1	13±2		11.9
M_4–N_6 (Mβ)	4.78±0.07	3.6±0.1	4.3±0.3	3.9±0.2	4.7
M_4–O_2	11±1				
M_4–O_6	18±2				
M_5–N_3	13.3±0.8	12.8±0.3	15±2		10.8
M_5–N_7 ($M\alpha_1$)	4.82±0.04[b]	3.5±0.1	4.1±0.3	3.8±0.2	4.5

The uncertainty intervals correspond to one standard deviation. Main complications for each determination: [a]Two satellite structures; [b]doublet and satellite band; [c]line distorted by M_5 absorption edge.
The results obtained in this work are compared with other determinations.

In order to calculate the angular divergence $\Delta\theta$, almost constant for the Johansson arrangement [19], the parameters γ_G obtained with the optimization algorithm for uranium, thorium, bismuth and lead Mβ lines, were fitted using the function given by Eq. (14). Finally, with the value obtained for $\Delta\theta$, the parameter γ_L was determined from the optimization process for twelve M uranium transitions. The corresponding natural linewidths ($2\gamma_L$) can be seen in the second column of Table 2 compared with other experimental and theoretical values. In the third column, results obtained by high-resolution X-ray spectroscopy are displayed [20]; the fourth column shows experimental values measured with PAX (photoelectron analysis of X-rays) [21]; and linewidths measured by high-resolution double crystal X-ray spectroscopy are presented in the fifth column [22]. The theoretical linewidths given in the sixth column were obtained by Raboud de Villarsiviriaux [20] by adding the widths of the M and N levels involved in each transition, taken from McGuire's predictions (Refs. [23] and [24], respectively).

The value for γ_L given by Keski-Rakhonen and Krause [21] for the Mγ line is indicated by these authors as distorted by the M_5 absorption edge. This inconvenience was overcome in this work by taking into account all the absorption edges involved in the prediction of the

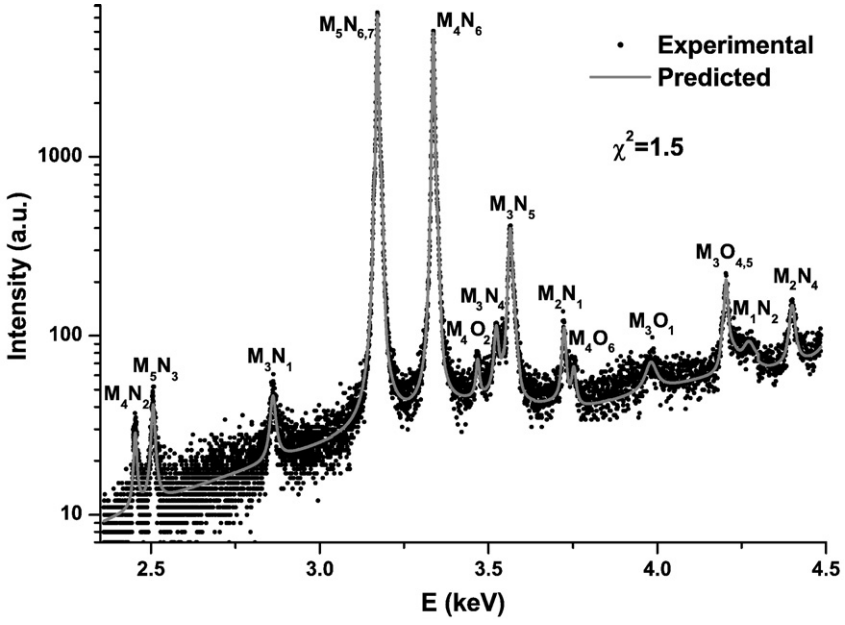

Fig. 3. Experimental and predicted X-ray spectrum of uranium. All the characteristic lines were fitted with the Voigt profile given by Eqs. (11) and (12).

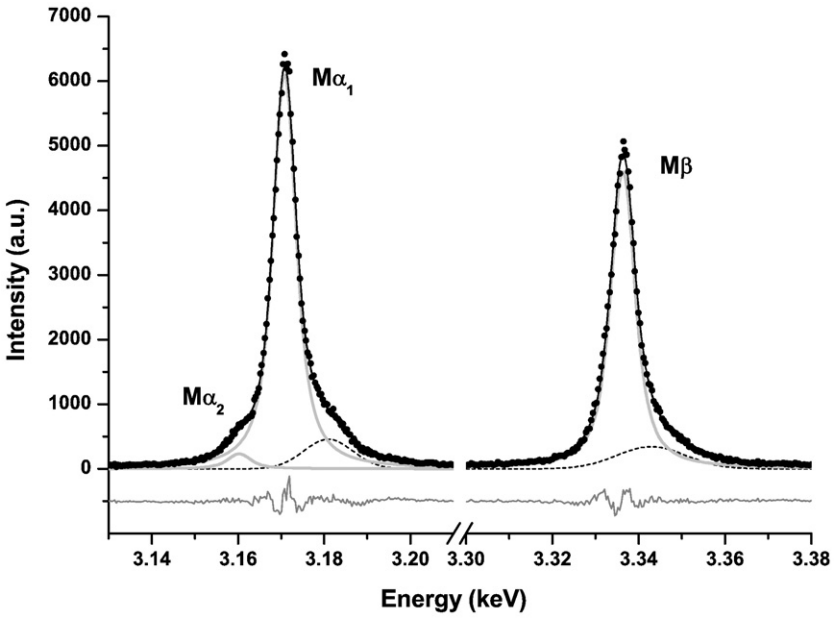

Fig. 4. Uranium spectrum in the region corresponding to the Mα and Mβ lines. Dots: experimental, black solid line: prediction, light grey thick solid lines: parent lines, dashed lines: satellite bands and grey thin solid lines: residuals.

spectrum $\tilde{I}$. Another problem arises in relation to this transition: between the Mγ and the M_3N_4 lines there is a broad structure that may be attributed to a M_5P_1 quadrupole transition, and several unresolved lines tentatively assigned to the M_3N_4 N satellite, to the M_4O_3 and to the M_5P_3 transitions [20]. It is almost impossible to perform a reliable fit of the M_3N_4 line because of that combination of problems; thus it was not included in Table 2. Another case difficult to deal for the present approach is the Mα doublet, since the two lines involved are overlapped with a satellite structure. The M_3O_1 line was not considered because it is extremely weak to yield a reliable value for γ_L.

The satellite bands at the high energy side of the $M\alpha_1$, Mβ, Mγ and M_3O_5 lines were fitted with Gaussian profiles with variable amplitudes and widths, centered at 10.1, 6.5, 11.0 and 11.0 eV from the parent line, respectively. The main mechanism in the generation of these bands is the emission of an N electron after a Coster–Kronig transition (CK) within the M shell. When the doubly ionized atom decays to fill the M vacancy, the energy levels are altered due to the N spectator hole and then, the characteristic photon is emitted with an energy slightly greater than the corresponding to the diagram line. The amount of the satellite shift depends on the shell to which the spectator hole belongs: between 7 and 10 eV for the $M\alpha_1$ and Mβ lines, according to theoretical calculations performed by Keski-Rahkonen and Krause. When the incident beam energy is sufficient to ionize the L shell, an Auger LMM decay leaving the atom in a double M vacancy state is possible; in this case, the distortion of levels is much stronger, producing a satellite shift of more than 50 eV. This case, however, is excluded in the present experiment, since the excitation energy is only 15 keV. Another mechanism of decay is the shake-off, for which a second electron is ejected from a more external shell (O, P or Q, for the heaviest elements) without CK transitions. This second vacancy distorts very weakly the atomic energy levels; thus, the characteristic photon completing the decay is emitted with an energy almost equal to that of the diagram line ($\Delta E < 1$ eV) from which is usually undistinguishable [22].

When a satellite band is present, the determination of the linewidth of the associated diagram line is influenced by the description of that satellite structure. The uranium experimental spectrum in the regions involving the Mα and Mβ lines is shown in Fig. 4 together with the fitting curve, the contributions of each line and the corresponding satellite bands. As mentioned above, the fitting method used in this work is based on a minimization process carried out in a wide spectral range. Raboud de Villarsiviriaux [20] performs the fitting in narrow spectral regions also by a minimization routine, although he includes one or two Voigt profiles without giving a clear justification of the criterion used in each case. Other authors, instead of fitting the satellite structure along with the parent lines, only fit the main lines and assign the residuals to the satellite band [21,22]. This strategy introduces a systematic overestimation in the diagram line intensity, since the low energy tail of the satellite structure is accounted for as a part of the main peak.

The results obtained in the present work are in agreement with the values given by other authors by considering the important discrepancies among them. The better experimental resolution related to the

Table 3
Coefficients required to calculate the product erfc(a) exp(a^2) given by Eq. (A1)

j	p	q	s	t
0	1.2303393547979725272E3	1.2303393548037494 2043E3	6.5874916152983780 3157E−4	2.3352049762686918 5443E−3
1	2.0510783778260714 6532E3	3.4393676741437216 3696E3	1.6083785148742276 6278E−2	6.0518341312441319 1178E−2
2	1.7120476126340705 8314E3	4.3626190901432471 582E3	0.12578172611122924 6204	0.52790510295142841 2248
3	8.8195222124176909 0411E2	3.2907992357334596 2678E3	0.360344899949804439429	1.87295284992346047209
4	2.9863513819740013 1132E2	1.6213895745666901 8874E3	0.305326634961232344035	2.56852019228982242072
5	66.11919063714162 94775	5.3718110186200985 7509E2	0.016315387137302 0978498	1.0
6	8.8831479438837594118	1.1769395089131249 9305E2		
7	0.56418849698867008918	15.7449261107098347253		
8	2.1531153547440384 6343E−8	1.0		

spectrometers used by those authors is not sufficient to obtain precise values for γ_L, since these natural linewidths are large enough to complicate the deconvolution in certain cases, particularly for peaks accompanied by satellite structures. Besides that, a good fitting method that take into account most of the fundamental and experimental processes in a realistic manner is necessary. In this sense, a parameter refinement method involving Voigt profiles for the description of the characteristic peaks, like the one implemented in the POEMA program [17], shows a good performance in this application.

5. Conclusion

A simple expression for the Voigt function was developed in terms of the complementary error function with complex arguments, which in turn, was expressed in terms of series of trigonometric and hyperbolic functions with real arguments. Far from the maximum, a very simple asymptotic expansion was used.

The proposed expression has an accuracy better than 10^{-8} within the studied range, which compares favorably with most of the algorithms available, and widely exceeds the requirements of spectroscopic applications. Moreover, the time per evaluation, of the order of tens of microseconds, results useful for the most stringent applications, which require billions of evaluations. In addition, all the tools necessary to implement the present algorithm are explicitly included in this work, which facilitates the use of the expression proposed. This approach was successfully implemented in an algorithm of atomic and instrumental parameter refinement in EPMA to describe the characteristic line profiles in an X-ray emission spectrum.

The natural widths of 12 characteristic uranium M lines were obtained with this methodology. The determination of these values is very important because they are scarce in the literature due to the theoretical and experimental difficulties related to the complexity of the more external shells. Reasonable agreement was found between our results and the available experimental and theoretical data, bearing in mind the large discrepancies among them. In addition, natural linewidths were provided for four transitions not previously determined up to our knowledge.

Acknowledgements

The authors wish to thank Dr. Alejo Carreras for his assistance in the measurement of the uranium spectrum used in this work.

Appendix A

The product $\mathrm{erfc}(a)\exp(a^2)$ used in Eq. (11) was evaluated according to the algorithm proposed by Cody [16].

$$\mathrm{erfc}(a)\exp(a^2) = \begin{cases} \dfrac{\sum_{j=0}^{8} p_j a^j}{\sum_{j=0}^{8} q_j a^j} & 0.46875 \le a \le 4 \\ \dfrac{1}{a}\left(\dfrac{1}{\sqrt{\pi}} - \dfrac{1}{a^2}\dfrac{\sum_{j=0}^{5} s_j a^{-2j}}{\sum_{j=0}^{5} t_j a^{-2j}}\right) & a \ge 4 \end{cases} \quad \text{(A1)}$$

For the purposes of the present work, the lower limit in the upper branch of Eq. (A1) was extended down to 0.01 keeping the required degree of accuracy.

The coefficients p_j, q_j, s_j and t_j are presented in Table 3.

References

[1] C. Fournier, C. Merlet, O. Dungne, M. Fialin, Standardless semi-quantitative analysis with WDS-EPMA, J. Anal. At. Spectrom. 14 (1999) 381–386.
[2] G. Rémond, R. Myklebust, M. Fialin, C. Nockolds, M. Phillips, C.R. Carmes, Decomposition of wavelength dispersive X-ray spectra, J. Res. Natl. Inst. Stand. Technol. 107 (2002) 509–529.
[3] T.C. Huang, G. Lim, Resolution of overlapping X-ray fluorescence peaks with the pseudo-Voigt function, Adv. X-Ray Anal. 29 (1986) 461–468.
[4] G. Rémond, J.L. Campbell, R.H. Packwood, M. Fialin, Spectral decomposition of wavelength dispersive X-ray spectra: implications for quantitative analysis in the electron probe microanalyzer, Scanning Microsc. (Suppl.7) (1993) 89–135.
[5] Y. Liu, J. Lin, G. Huang, Y. Guo, C. Duan, Simple empirical analytical approximation to the Voigt profile, J. Opt. Soc. Am. B 18 (2001) 666–672.
[6] J.F. Kielkopf, New approximation to the Voigt function with applications to spectral-line profile analysis, J. Opt. Soc. Am. 63 (1973) 987–995.
[7] S.R. Drayson, Rapid computation of the Voigt profile, J. Quant. Spectrosc. Radiat. Transfer 16 (1976) 611–614.
[8] W.J. Thompson, Numerous neat algorithms for the Voigt profile function, Comput. Phys. 7 (1993) 627–631.
[9] A. Brablec, D. Trunec, F. Stastny, Deconvolution of spectral line profiles: solution of the inversion problem, Phys. Rev. D: Part., Fields, Gravitation, Cosmol. 32 (1999) 1870–1875.
[10] H.O. Di Rocco, The exact expression of the Voigt profile function, J. Quant. Spectrosc. Radiat. Transfer 92 (2005) 231–237.
[11] H.O. Di Rocco, D.I. Iriarte, J.A. Pomarico, General expression for the Voigt function that is of special interest for applied spectroscopy, Appl. Spectrosc. 55 (2001) 822–826.
[12] G.D. Roston, F.S. Obaid, Exact analytical formula for Voigt spectral line profile, J. Quant. Spectrosc. Radiat. Transfer 94 (2005) 255–263.
[13] T. Andersen, The differential equations of the Voigt function, J. Quant. Spectrosc. Radiat. Transfer 19 (1978) 169–171.
[14] M.R. Zaghloul, On the calculation of the Voigt profile: a single proper integral with a damped sine integrand, Mon. Not. R. Astron. Soc. 375 (2007) 1043–1048.
[15] M. Abramowitz, I.A. Stegun, Handbook of Mathematical Functions, Ninth printing, Dowe Publications, Inc., New York, 1970, p. 299.
[16] W.J. Cody, Rational Chebyshev approximation for the error function, Math. Comput. 23 (1969) 631–637.
[17] R. Bonetto, G. Castellano, J. Trincavelli, Optimization of parameters in electron probe microanalysis, X-Ray Spectrom. 30 (2001) 313–319.
[18] H.O. Di Rocco, M. Aguirre Téllez, Evaluation of the asymmetric Voigt profile and complex error functions in terms of the Kummer functions, Acta Phys. Pol., A 106 (2004) 817–826.
[19] S. Reed, Electron Microprobe Analysis, 2nd Ed., Cambridge University Press, Cambridge, 1993, pp. 71–74.
[20] P. Raboud de Villarsiviriaux, Ph. D. Thesis, Université de Fribourg, Switzerland (2001).
[21] O. Keski-Rahkonen, M. Krause, Uranium M X-ray emission spectrum, Phys. Rev., A At. Mol. Opt. Phy. 15 (1977) 959–966.
[22] M. Ohno, A. Laakkonen, A. Vuoristo, G. Graeffe, High resolution M X-ray spectrum of metallic uranium (Z=92), Phys. Scr. 34 (1986) 146–150.
[23] E. McGuire, in: R. Flink, S. Manson, J. Palms, P. Rao (Eds.), Proceedings of the International Conference on Inner Shell Ionization Phenomena and Future Applications, Atlanta, U.S., 1972, Natl. Tech. Information Service, U. S. Dept. of Commerce, Springfield, Va, 1973, p. 662, CONF-720404.
[24] E. McGuire, Atomic N-shell Coster–Kronig, Auger and radiative rates and fluorescence yields for 38≤Z≤103, Phys. Rev., A At. Mol. Opt. Phy. 9 (1974) 1840–1851.
[25] K. Letchworth, D. Benner, Rapid and accurate calculation of the Voigt function, J. Quant. Spectrosc. Radiat. Transfer 107 (2007) 173–192.
[26] A. Hui, B. Armstrong, A. Wray, Rapid computation of the Voigt and complex error functions, J. Quant. Spectrosc. Radiat. Transfer 19 (1978) 509–516.
[27] J. Trincavelli, G. Castellano, R. Bonetto, L-shell transition rates for Ba, Ta, W, Pt, Pb and Bi using electron microprobe, Spectrochim. Acta Part B 57 (2002) 919–928.
[28] J. Trincavelli, S. Limandri, A. Carreras, R. Bonetto, Experimental method to determine the absolute efficiency curve of a wavelength dispersive spectrometer, Microsc. Microanal. 14 in press.